A Combined $\nu_\mu \to \nu_e$ & $\bar{\nu}_\mu \to \bar{\nu}_e$ Oscillation Analysis of the MiniBooNE Excesses

A. A. Aguilar-Arevalo[12], B. C. Brown[6], L. Bugel[11], G. Cheng[5], E. D. Church[15], J. M. Conrad[11], R. Dharmapalan[1], Z. Djurcic[2], D. A. Finley[6], R. Ford[6], F. G. Garcia[6], G. T. Garvey[9], J. Grange[7], W. Huelsnitz[9], C. Ignarra[11], R. Imlay[10], R. A. Johnson[3], G. Karagiorgi[5], T. Katori[11], T. Kobilarcik[6], W. C. Louis[9], C. Mariani[5], W. Marsh[6], G. B. Mills[9], J. Mirabal[9], C. D. Moore[6], J. Mousseau[7], P. Nienaber[14], B. Osmanov[7], Z. Pavlovic[9], D. Perevalov[6], C. C. Polly[6], H. Ray[7], B. P. Roe[13], A. D. Russell[6], M. H. Shaevitz[5], J. Spitz[11], I. Stancu[1], R. Tayloe[8], R. G. Van de Water[9], D. H. White[9], D. A. Wickremasinghe[3], G. P. Zeller[6], E. D. Zimmerman[4]

(The MiniBooNE Collaboration)

[1] *University of Alabama; Tuscaloosa, AL 35487*
[2] *Argonne National Laboratory; Argonne, IL 60439*
[3] *University of Cincinnati; Cincinnati, OH 45221*
[4] *University of Colorado; Boulder, CO 80309*
[5] *Columbia University; New York, NY 10027*
[6] *Fermi National Accelerator Laboratory; Batavia, IL 60510*
[7] *University of Florida; Gainesville, FL 32611*
[8] *Indiana University; Bloomington, IN 47405*
[9] *Los Alamos National Laboratory; Los Alamos, NM 87545*
[10] *Louisiana State University; Baton Rouge, LA 70803*
[11] *Massachusetts Institute of Technology; Cambridge, MA 02139*
[12] *Instituto de Ciencias Nucleares, Universidad Nacional Autónoma de México, D.F. 04510, México*
[13] *University of Michigan; Ann Arbor, MI 48109*
[14] *Saint Mary's University of Minnesota; Winona, MN 55987*
[15] *Yale University; New Haven, CT 06520*

(Dated: August 28, 2012)

The MiniBooNE experiment at Fermilab reports results from an analysis of the combined ν_e and $\bar{\nu}_e$ appearance data from 6.46×10^{20} protons on target in neutrino mode and 11.27×10^{20} protons on target in antineutrino mode. A total excess of $240.3 \pm 34.5 \pm 52.6$ events (3.8σ) is observed from combining the two data sets in the energy range $200 < E_\nu^{QE} < 1250$ MeV. In a combined fit for CP-conserving $\nu_\mu \to \nu_e$ and $\bar{\nu}_\mu \to \bar{\nu}_e$ oscillations via a two-neutrino model, the background-only fit has a χ^2-probability of 0.03% relative to the best oscillation fit. The data are consistent with neutrino oscillations in the $0.01 < \Delta m^2 < 1.0$ eV^2 range and with the evidence for antineutrino oscillations from the Liquid Scintillator Neutrino Detector (LSND).

There is growing evidence for short-baseline neutrino anomalies occuring at an $L/E_\nu \sim 1$ m/MeV, where E_ν is the neutrino energy and L is the distance that the neutrino travelled before detection. These anomalies include the excess of events observed by the LSND [1] and MiniBooNE [2–4] experiments and the deficit of events observed by reactor [5] and radioactive-source experiments [6]. There have been several attempts to interpret these anomalies in terms of 3+N neutrino oscillation models involving three active neutrinos and N additional sterile neutrinos [7–12]. (Other more exotic explanations include, for example, Lorentz violation [13] and sterile neutrino decay [14].) This paper presents a combined oscillation analysis of the MiniBooNE ν_e and $\bar{\nu}_e$ appearance data, corresponding to 6.46×10^{20} protons on target (POT) in neutrino mode [3] and 11.27×10^{20} POT in antineutrino mode, which is approximately twice the antineutrino data reported previously [4].

This analysis fits both $\nu_\mu \to \nu_e$ and $\bar{\nu}_\mu \to \bar{\nu}_e$ oscillations with the same oscillation model over the full neutrino energy range $200 < E_\nu^{QE} < 3000$ MeV, where E_ν^{QE} is the reconstructed neutrino energy assuming quasielastic scattering kinematics [15]. The neutrino oscillation energy region is defined to be $200 < E_\nu^{QE} < 1250$ MeV, which is where an LSND-like signal (same L/E_ν) is expected. Combining neutrino and antineutrino data over the full energy range has the advantage of decreasing statistical and systematic errors. The analysis assumes no significant ν_μ, $\bar{\nu}_\mu$, ν_e, or $\bar{\nu}_e$ disappearance. This simplification may change the fitted $\nu_\mu \to \nu_e$ and $\bar{\nu}_\mu \to \bar{\nu}_e$ appearance probabilities by up to $\sim 20\%$. Furthermore, it has been suggested that nuclear effects associated with neutrino interactions on carbon can affect the reconstruction of the neutrino energy and the determination of the neutrino oscillation parameters [16]. These effects are not fully accounted for in the analysis and may affect somewhat the oscillation fit parameters discussed below.

The neutrino (antineutrino) flux is produced by 8 GeV protons from the Fermilab Booster interacting on a beryllium target inside a magnetic focusing horn set at positive (negative) polarity. In neutrino (antineutrino) mode, positively (negatively) charged mesons produced in p-Be

interactions are focused in the forward direction and subsequently decay primarily into ν_μ ($\bar{\nu}_\mu$). The flux of neutrinos and antineutrinos of all flavors is simulated using information from external measurements [17]. In neutrino mode, the ν_μ, $\bar{\nu}_\mu$, ν_e, and $\bar{\nu}_e$ flux contributions at the detector are 93.5%, 5.9%, 0.5%, and 0.1%, respectively. In antineutrino mode, the $\bar{\nu}_\mu$, ν_μ, $\bar{\nu}_e$, and ν_e flux contributions at the detector are 83.7%, 15.7%, 0.4%, and 0.2%, respectively. The ν_μ and $\bar{\nu}_\mu$ fluxes peak at approximately 600 MeV and 400 MeV, respectively.

The MiniBooNE detector is described in detail in reference [18]. The detector is located 541 m from the beryllium target and consists of a 40-foot diameter sphere filled with 806 tons of pure mineral oil (CH_2). Neutrino interactions in the detector produce charged particles (electrons, muons, protons, pions, and kaons) which in turn produce scintillation and Cherenkov light detected by the 1520 8-inch photomultiplier tubes (PMTs) that line the interior of the detector and an optically isolated outer veto region. Event reconstruction and particle identification are derived from the hit PMT charge and time information.

The signature of $\nu_\mu \to \nu_e$ and $\bar{\nu}_\mu \to \bar{\nu}_e$ oscillations is an excess of ν_e and $\bar{\nu}_e$-induced charged-current quasi-elastic (CCQE) events. Reconstruction [19] and selection requirements of these events are almost identical to those from previous analyses [3, 4] with an average reconstruction efficiency of $\sim 10-15\%$ for events generated over the entire volume of the detector. Recent improvements to the analysis include a better determination of the intrinsic ν_e background from K^+ decay through the measurement of high-energy neutrino events in the SciBooNE experiment [20], a combined error matrix for neutrino and antineutrino data with correlated and uncorrelated errors, a better determination of neutral-current π^0 and external event background in antineutrino mode due to the increase in statistics of the antineutrino mode data sample, and the use of a likelihood fit with frequentist corrections from fake data studies for both the neutrino-mode and antineutrino-mode data. The detector cannot distinguish between neutrino and antineutrino interactions on an event-by-event basis. However, the fraction of CCQE events in antineutrino (neutrino) mode that are due to wrong-sign neutrino (antineutrino) events was determined from the angular distributions of muons created in CCQE interactions and by measuring charged-current single π^+ events [21].

The predicted ν_e and $\bar{\nu}_e$ CCQE background events for the neutrino oscillation energy range $200 < E_\nu^{QE} < 1250$ MeV are shown in Table I for both neutrino mode and antineutrino mode. The predicted backgrounds to the ν_e and $\bar{\nu}_e$ CCQE sample are constrained by measurements in MiniBooNE and include neutral current (NC) π^0 events [22] with photonuclear interactions, $\Delta \to N\gamma$ radiative decays [23], and neutrino interactions external to the detector. Other backgrounds from mis-identified ν_μ or $\bar{\nu}_\mu$ [24, 25] and from intrinsic ν_e and $\bar{\nu}_e$ events from the $\pi \to \mu$ decay chain are constrained and obtain their normalizations from the ν_μ and $\bar{\nu}_\mu$ CCQE data samples, which consist of 115,467 (50,456) events in neutrino (antineutrino) mode in the $200 < E_\nu^{QE} < 1900$ MeV energy range.

TABLE I: *The expected (unconstrained) number of events for the $200 < E_\nu^{QE} < 1250$ MeV neutrino oscillation energy range from all of the backgrounds in the ν_e and $\bar{\nu}_e$ appearance analysis and for the LSND expectation of 0.26% oscillation probability averaged over neutrino energy for both neutrino mode and antineutrino mode.*

Process	Neutrino Mode	Antineutrino Mode
ν_μ & $\bar{\nu}_\mu$ CCQE	37.1	12.9
NC π^0	252.3	112.3
NC $\Delta \to N\gamma$	86.8	34.7
External Events	35.3	15.3
Other ν_μ & $\bar{\nu}_\mu$	45.1	22.3
ν_e & $\bar{\nu}_e$ from $\mu^\pm$ Decay	214.0	91.4
ν_e & $\bar{\nu}_e$ from $K^\pm$ Decay	96.7	51.2
ν_e & $\bar{\nu}_e$ from K^0_L Decay	27.4	51.4
Other ν_e & $\bar{\nu}_e$	3.0	6.7
Total Background	797.7	398.2
0.26% $\bar{\nu}_\mu \to \bar{\nu}_e$	233.0	100.0

Systematic uncertainties are determined by considering the predicted effects on the ν_μ, $\bar{\nu}_\mu$, ν_e, and $\bar{\nu}_e$ CCQE rate from variations of actual parameters. These include uncertainties in the neutrino and antineutrino flux estimates, uncertainties in neutrino cross sections, most of which are determined by in situ cross-section measurements at MiniBooNE, and uncertainties in detector modeling and reconstruction. A covariance matrix in bins of E_ν^{QE} is constructed by considering the variation from each source of systematic uncertainty on the ν_e and $\bar{\nu}_e$ CCQE signal, background, and ν_μ and $\bar{\nu}_\mu$ CCQE prediction as a function of E_ν^{QE}. This matrix includes correlations between any of the ν_e and $\bar{\nu}_e$ CCQE signal and background and ν_μ and $\bar{\nu}_\mu$ CCQE samples, and is used in the χ^2 calculation of the oscillation fit.

Fig. 1 shows the E_ν^{QE} distribution for ν_e and $\bar{\nu}_e$ CCQE data and background in neutrino and antineutrino mode over the full available energy range. Each bin of reconstructed E_ν^{QE} corresponds to a distribution of "true" generated neutrino energies, which can overlap adjacent

TABLE II: *The number of data, fitted (constrained) background, and excess events in the ν_e and $\bar{\nu}_e$ analyses for neutrino mode, antineutrino mode, and combined in the neutrino oscillation energy range $200 < E_\nu^{QE} < 1250$ MeV. The uncertainties include both statistical and constrained systematic errors. All known systematic errors are included in the systematic error estimate.*

Mode	Data	Background	Excess
Neutrino Mode	952	$790.0 \pm 28.1 \pm 38.7$	162.0 ± 47.8
Antineutrino Mode	478	$399.6 \pm 20.0 \pm 20.3$	78.4 ± 28.5
Combined	1430	$1189.7 \pm 34.5 \pm 52.6$	240.3 ± 62.9

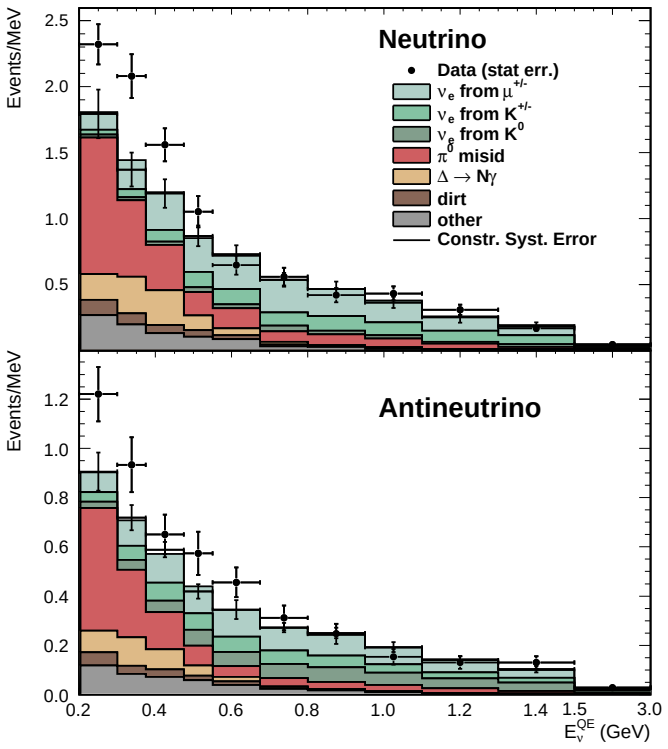

FIG. 1: The neutrino mode (top) and antineutrino mode (bottom) E_ν^{QE} distributions for ν_e CCQE data (points with statistical errors) and background (histogram with systematic errors).

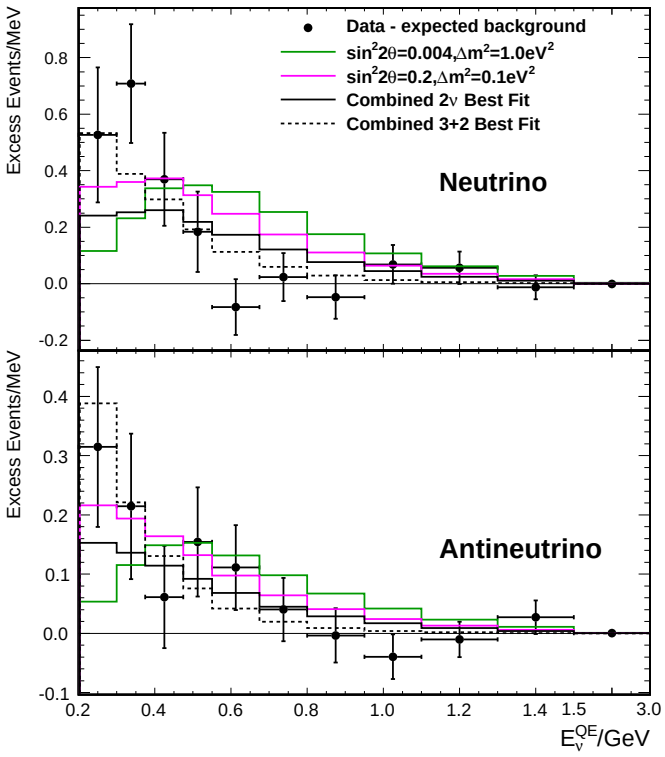

FIG. 2: The neutrino mode (top) and antineutrino mode (bottom) event excesses as a function of E_ν^{QE}. Also shown are the expectations from the best two-neutrino and 3+2 joint oscillation fits with $200 < E_\nu^{QE} < 3000$ MeV and from two reference values in the LSND allowed region. All known systematic errors are included in the systematic error estimate.

bins. In neutrino (antineutrino) mode, a total of 952 (478) events pass the ν_e event selection requirements with $200 < E_\nu^{QE} < 1250$ MeV, compared to an expectation of $790.0 \pm 28.1 \pm 38.7$ ($399.6 \pm 20.0 \pm 20.3$) events, where the first error is statistical and the second error is systematic. This corresponds to a neutrino (antineutrino) excess of 162.0 ± 47.8 (78.4 ± 28.5) events. Combining the data in neutrino mode and antineutrino mode, the total excess is 240.3 ± 62.9 events. Fig. 2 shows the event excesses as a function of E_ν^{QE} in both neutrino and antineutrino modes. The number of data, fitted background, and excess events for neutrino mode, antineutrino mode, and combined are summarized in Table II.

Many checks have been performed on the data, including beam and detector stability checks that show that the neutrino event rates are stable to $< 2\%$ and that the detector energy response is stable to $< 1\%$ over the entire run. In addition, the fractions of neutrino and antineutrino events are stable over energy and time, and the inferred external event rate corrections are similar in both neutrino and antineutrino modes.

A comparison between the MiniBooNE and LSND antineutrino data sets is given in Fig. 3, which shows the oscillation probability as a function of L/E_ν for $\nu_\mu \rightarrow \nu_e$ and $\bar{\nu}_\mu \rightarrow \bar{\nu}_e$ candidate events in the L/E_ν range where MiniBooNE and LSND overlap. The data used for LSND and MiniBooNE correspond to $20 < E_\nu < 60$ MeV and $200 < E_\nu^{QE} < 3000$ MeV, respectively. The oscillation probability is defined as the event excess divided by the number of events expected for 100% $\nu_\mu \rightarrow \nu_e$ and $\bar{\nu}_\mu \rightarrow \bar{\nu}_e$ transmutation in each bin, while L is the distance travelled by the neutrino or antineutrino from the mean neutrino production point to the detector and E_ν is the reconstructed neutrino or antineutrino energy. The largest oscillation probabilities from both LSND and MiniBooNE occur at $L/E_\nu \geq 1$ m/MeV.

The MiniBooNE data are next fit to a two-neutrino oscillation model, where the probability, P, of $\nu_\mu \rightarrow \nu_e$ and $\bar{\nu}_\mu \rightarrow \bar{\nu}_e$ oscillations is given by $P = \sin^2 2\theta \sin^2(1.27\Delta m^2 L/E_\nu)$, $\sin^2 2\theta = 4|U_{e4}|^2|U_{\mu 4}|^2$, and $\Delta m^2 = \Delta m^2_{41} = m^2_4 - m^2_1$. The oscillation parameters are extracted from a combined fit to the ν_e, $\bar{\nu}_e$, ν_μ, and $\bar{\nu}_\mu$ CCQE event distributions. The fit assumes CP conservation with the same oscillation probability for neutrinos and antineutrinos, including both right-sign and wrong-sign neutrinos, and no significant ν_μ, $\bar{\nu}_\mu$, ν_e, or $\bar{\nu}_e$ disappearance. Using a likelihood-ratio technique [4], the best oscillation fit for $200 < E_\nu^{QE} < 3000$ MeV occurs at

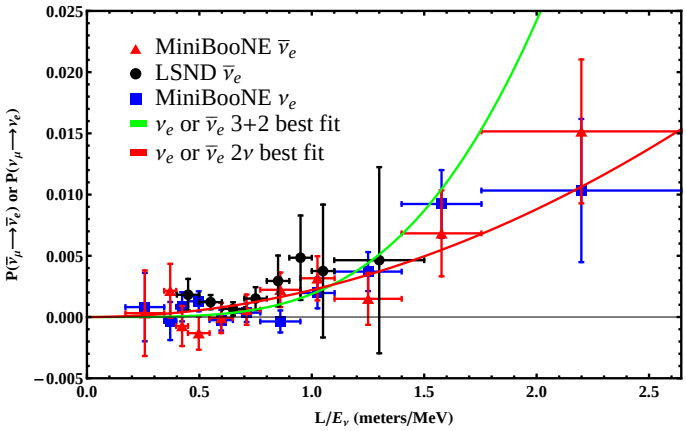

FIG. 3: The oscillation probability as a function of L/E_ν^{QE} for $\nu_\mu \to \nu_e$ and $\bar{\nu}_\mu \to \bar{\nu}_e$ candidate events from MiniBooNE and $\bar{\nu}_\mu \to \bar{\nu}_e$ candidate events from LSND. The data points include both statistical and systematic errors. Also shown are the oscillation probabilities from the two-neutrino and 3+2 joint oscillation fits.

$(\Delta m^2, \sin^2 2\theta) = (0.037\ \text{eV}^2, 1.00)$. The χ^2/ndf for the best-fit point in the neutrino oscillation energy range of $200 < E_\nu^{QE} < 1250$ MeV is 24.7/15.6, corresponding to a probability of 6.7%. The probability of the background-only fit relative to the best oscillation fit is 0.03%. Fig. 4 shows the MiniBooNE closed contours for ν_e and $\bar{\nu}_e$ appearance oscillations in neutrino mode and antineutrino mode separately in the $200 < E_\nu^{QE} < 3000$ MeV energy range, where a two-neutrino oscillation model is assumed and where frequentist studies were performed to determine the confidence level (C.L.) regions. The separate best fits for neutrino mode and antineutrino mode are at $(\Delta m^2, \sin^2 2\theta)$ values of $(3.14\ \text{eV}^2, 0.002)$ and $(0.05\ \text{eV}^2, 0.842)$. In the neutrino oscillation energy range of $200 < E_\nu^{QE} < 1250$ MeV, the χ^2/ndf for the best-fit points in neutrino mode and antineutrino mode are 13.2/6.8 and 4.8/6.9 with probabilities of 6.1% and 67.5%, respectively. The background-only fit has a χ^2-probability of 1.6% and 0.5% relative to the best oscillation fits for neutrino and antineutrino, respectively. Fig. 5 shows the closed contours for the combined fit. The allowed regions for $\Delta m^2 < 1\ \text{eV}^2$ are in agreement with the LSND allowed region [1] and consistent with the limits from the KARMEN experiment [26]. Fig. 2 shows the expectations from both the best two-neutrino joint oscillation fit and from a 3+2 joint oscillation fit as a function of E_ν^{QE} in both neutrino and antineutrino modes. The best-fit parameters from the 3+2 oscillation fit are $\Delta m^2_{41} = 0.082\ \text{eV}^2$, $\Delta m^2_{51} = 0.476\ \text{eV}^2$, $|U_{e4}|^2|U_{\mu 4}|^2 = 0.1844$, $|U_{e5}|^2|U_{\mu 5}|^2 = 0.00547$, and $\phi = 1.0005\pi$. The 3+2 fit has three more parameters than the two-neutrino fit [12] and will be discussed in a future publication.

In summary, the MiniBooNE experiment observes a total excess of 240.3 ± 62.9 ν_e and $\bar{\nu}_e$ events (3.8σ) in

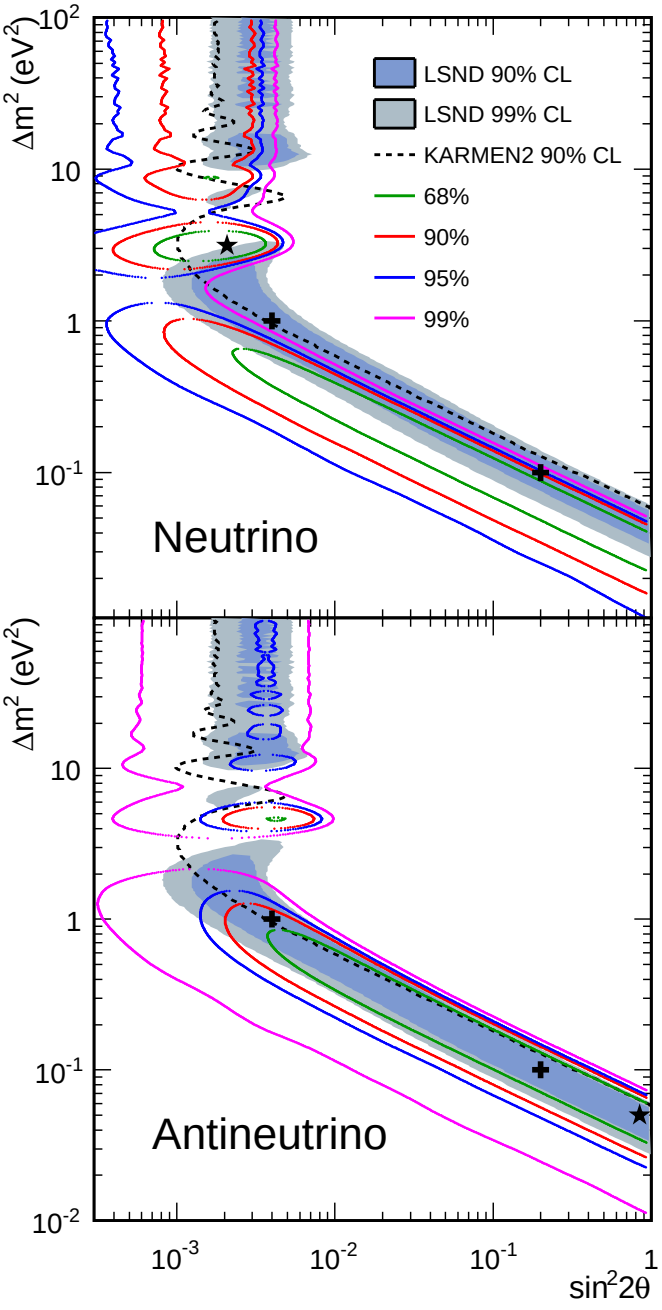

FIG. 4: MiniBooNE allowed regions in neutrino mode (top) and antineutrino mode (bottom) for events with $E_\nu^{QE} > 200$ MeV within a two-neutrino $\nu_\mu \to \nu_e$ and $\bar{\nu}_\mu \to \bar{\nu}_e$ oscillation model. Also shown is the $\bar{\nu}_\mu \to \bar{\nu}_e$ limit from the KARMEN experiment [26]. The shaded areas show the 90% and 99% C.L. LSND $\bar{\nu}_\mu \to \bar{\nu}_e$ allowed regions. The black stars show the best fit points, while the crosses show LSND reference values.

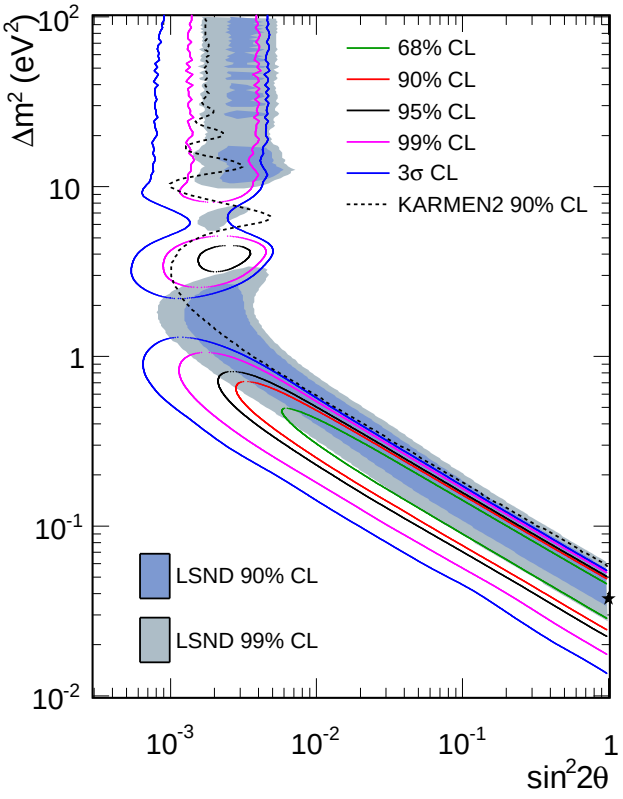

FIG. 5: MiniBooNE allowed regions in combined neutrino and antineutrino mode for events with $200 < E_\nu^{QE} < 3000$ MeV within a two-neutrino $\nu_\mu \to \nu_e$ and $\bar{\nu}_\mu \to \bar{\nu}_e$ oscillation model. Also shown is the $\bar{\nu}_\mu \to \bar{\nu}_e$ limit from the KARMEN experiment [26]. The shaded areas show the 90% and 99% C.L. LSND $\bar{\nu}_\mu \to \bar{\nu}_e$ allowed regions. The black star shows the best fit point.

the neutrino oscillation energy range $200 < E_\nu^{QE} < 1250$ MeV. The allowed regions from a two-neutrino fit to the data, shown in Fig. 5, are consistent with $\nu_\mu \to \nu_e$ and $\bar{\nu}_\mu \to \bar{\nu}_e$ oscillations in the 0.01 to 1 eV^2 Δm^2 range and consistent with the allowed region reported by the LSND experiment [1].

We acknowledge the support of Fermilab, the Department of Energy, and the National Science Foundation, and we acknowledge Los Alamos National Laboratory for LDRD funding.

[1] C. Athanassopoulos *et al.*, Phys. Rev. Lett. 75, 2650 (1995); 77, 3082 (1996); 81, 1774 (1998); Phys. Rev. C. **58**, 2489 (1998); A. Aguilar *et al.*, Phys. Rev. D 64, 112007 (2001).
[2] A. Aguilar-Arevalo *et al.*, Phys. Rev. Lett. 98, 231801 (2007).
[3] A. A. Aguilar-Arevalo *et al.*, Phys. Rev. Lett. 102, 101802 (2009).
[4] A. Aguilar-Arevalo *et al.*, Phys. Rev. Lett. 105, 181801 (2010).
[5] G. Mention, M. Fechner, T. Lasserre, T. A. Mueller, D. Lhuillier, M. Cribier, and A. Letourneau, Phys. Rev. D 83, 073006 (2011).
[6] C. Giunti and M. Laveder, Phys. Rev. C 83, 065504 (2011).
[7] M. Sorel, J. M. Conrad and M. H. Shaevitz, Phys. Rev. D 70, 073004 (2004).
[8] G. Karagiorgi, Z. Djurcic, J. M. Conrad, M. H. Shaevitz and M. Sorel, Phys. Rev. D 80, 073001 (2009) [Erratum-ibid. D 81, 039902 (2010)].
[9] C. Giunti and M. Laveder, Phys. Lett. B 706, 200 (2011); Phys. Rev. D84, 073008, (2011).
[10] J. Kopp, M. Maltoni and T. Schwetz, Phys. Rev. Lett. 107, 091801 (2011).
[11] K. N. Abazajian et al., arXiv:1204.5379 [hep-ph] (2012).
[12] J. M. Conrad, C. M. Ignarra, G. Karagiorgi, M. H. Shaevitz, and J. Spitz, arXiv:1207.4765 [hep-ex] (2012).
[13] V. A. Kostelecky and M. Mewes, Phys. Rev. D 69, 016005 (2004); T. Katori *et al.*, Phys. Rev. D 74, 105009 (2006).
[14] S. N. Gninenko, Phys. Rev. Lett. 99, 261601 (2007); S. N. Gninenko and D. S. Gorbunov, Phys. Rev. D 81, 075013 (2010).
[15] A. A. Aguilar-Arevalo *et al.*, Phys. Rev. D 81, 092005 (2010).
[16] M. Martini, M. Ericson, and G. Chanfray, arXiv:1202.4745 [hep-ph] (2012); J. Nieves, F. Sanchez, I. Ruiz Simo, and M. J. Vicente Vacas, arXiv:1204.5404 [hep-ph] (2012); O. Lalakulich and U. Mosel, arXiv:1208.3678 [nucl-th] (2012).
[17] A. A. Aguilar-Arevalo *et al.*, Phys. Rev. D 79, 072002 (2009).
[18] A. A. Aguilar-Arevalo *et al.*, Nucl. Instrum. Meth. A 599, 28 (2009).
[19] R. B. Patterson *et al.*, Nucl. Instrum. Meth. A 608, 206 (2009).
[20] G. Cheng *et al.*, Phys. Rev. D84, 012009 (2011).
[21] A. A. Aguilar-Arevalo *et al.*, Phys. Rev. D 84, 072002 (2011).
[22] A. A. Aguilar-Arevalo *et al.*, Phys. Lett. B. 664, 41 (2008); Phys. Rev. D 81, 013005 (2010).
[23] J. P. Jenkins and T. Goldman, Phys. Rev. D 80, 053005 (2009); Richard J. Hill, Phys. Rev. D 81, 013008 (2010); Brian D. Serot and Xilin Zhang, arXiv:1206.3812 [nucl-th] (2012); arXiv:1206.6324 [nucl-th] (2012); arXiv:1208.1553 [nucl-th] (2012).
[24] A. A. Aguilar-Arevalo *et al.*, Phys. Rev. Lett. 100, 032301 (2008).
[25] A. A. Aguilar-Arevalo *et al.*, Phys. Rev. Lett. 103, 081801 (2009).
[26] B. Armbruster *et al.*, Phys. Rev. D 65, 112001 (2002).